Ion induced field screening governs the early performance degradation of perovskite solar cells

Jarla Thiesbrummel
University of Oxford
Sahil Shah
University of Potsdam
Emilio Gutierrez-Partida
University of Potsdam
Fengshuo Zu
Humboldt-Universität
Francisco Camargo
University of Potsdam
Stefan Zeiske
Swansea University
Jonas Diekmann
University of Potsdam
Fangyuan Ye
East China University of Science and Technology
Karol Peters
University of Potsdam
Kai Brinkmann
University of Wuppertal https://orcid.org/0000-0002-2124-3904
Jonathan Warby
University of Potsdam
Quentin Jeangros
Centre Suisse d'Electronique et de Microtechnique
Felix Lang
University of Potsdam
Yongzhen Wu
East China University of Science and Technology https://orcid.org/0000-0003-3000-403X
Steve Albrecht
Helmholtz Zentrum Berlin
Thomas Riedl
Bergische Universitaet Wuppertal https://orcid.org/0000-0003-1084-316X
Ardalan Armin

Swansea University https://orcid.org/0000-0002-6129-5354
Dieter Neher
University of Potsdam https://orcid.org/0000-0001-6618-8403
Norbert Koch
Humboldt University of Berlin https://orcid.org/0000-0002-6042-6447
Vincent Corre
Friedrich-Alexander-Universität Erlangen-Nürnberg
Henry Snaith
University of Oxford https://orcid.org/0000-0001-8511-790X
Martin Stolterfoht (stolterf@uni-potsdam.de)
University of Potsdam https://orcid.org/0000-0002-4023-2178

Article

Keywords:

Posted Date: January 20th, 2023

DOI: https://doi.org/10.21203/rs.3.rs-2495973/v1

Abstract

In the last decade, perovskite semiconductors have triggered a revolution in solar cell research. However, critical issues remain concerning the stability of metal-halide perovskites, which need to be overcome to enable a large scale commercialisation of perovskite photovoltaics (PV). While the rather poor environmental stability of these perovskites is usually attributed to their ionic nature rendering them sensitive to moisture and oxygen, the actual contribution of mobile ions to the total degradation loss under different environmental conditions is poorly understood. In this work, we reveal that the initial degradation of perovskite semiconductors is largely the result of mobile ion-induced internal field screening - a phenomenon that has not been previously discussed in relation to the degradation of perovskite solar cells. The increased field screening leads to a decrease in the steady-state power conversion efficiency mainly due to a large reduction in current density, while the efficiency at high scan speeds (>1000 V/s) where the ions are immobilized is much less affected. We also show that interfacial recombination does not increase upon ageing, yet the open-circuit voltage (VOC) decreases as the result of an increase in the mobile ion density upon ageing. Furthermore, similar ionic losses appear under different external stressors, in particular when there are free charges present in the absorber layer. This work reveals a key degradation mechanism, providing new insights into initial device degradation before chemical or extrinsic mechanical device degradation effects manifest, and it highlights the critical role mobile ions play therein.

Introduction

Despite the impressive progress in terms of photovoltaic performance of perovskite solar cells over the last decade there still remain many issues regarding the stability. This has considerable implications for their real-world energy yield, and the levelized cost of electricity.[1–3] These challenges include various degradation pathways including material decomposition under light,[4,5] heat,[6,7] oxygen[8,9], and humidity[10,11] and a combination thereof. Efforts to improve device stability include, amongst many others, compositional engineering, e.g. omission of methylammonium iodide,[12,13] the use of additives,[14,15] transport layer (TL)[16–18] and interface engineering,[19] using a mixture of 2D and 3D perovskites,[20–22] the incorporation of diffusion barriers to the metal electrode (e.g. SnO_2,[23–25] CuSCN,[26] or bismuth[27]) and more effective encapsulation methods.[28] However, the stability reported in the academic literature remains far below the targeted values required for commercial viability (IEC standards and > 25 years operational lifetime). It is thus essential to gain a more comprehensive understanding of the underlying chemical and physical processes occurring during device ageing, and their effects on device performance.

In general, perovskites can also degrade over time without the presence of a specific external stressor, for example, due to strain within the material,[29,30] which leads to a reduced shelf lifetime. Other challenges related to perovskite-based tandem photovoltaics include the phase segregation in mixed-halide Br-rich perovskites[31–34] as well as mechanical concerns, for example, instabilities on top of (textured) Si

substrates due strain and potential delamination of charge transport and contact materials.[35] However, many of the intrinsic stability limitations are related to the presence of mobile ions in the perovskite layer, which behaves like a solid electrolyte with low-activation energies for ionic transport.[36] For methylammonium lead iodide (MAPI), density functional theory simulations have predicted a mobile ion density of $1x10^{19}$ cm^{-3} due to the low activation energy of the mobile ions (≈ 100 meV).[37] However, from an experimental and numerical perspective, such high mobile ion densities are very difficult to reconcile in well-performing devices and are controversial with most recent works narrowing the mobile ions density to $1x10^{15}$- $1x10^{17}$ cm^{-3} in devices with low levels of hysteresis.[38–42] Halide vacancies and interstitial iodine are usually considered to be the dominant species of mobile ions and they are particularly harmful since they can form I_2 - a solid that easily sublimes above room temperature, leading to a loss of absorber layer material, potentially causing electrode cracks and a critical device failure.[43] The migration and accumulation of halide defects due to lateral variation in the electric field also triggers the degradation of laboratory-scale solar cells at their edges and at the position of external impurities.[44] The formation of halide vacancies has also been linked to oxidation reactions at transport layers and metal electrodes.[45] Moreover, mobile ions and vacancies on both the A-site cations and the X-site halides have been shown to be able to diffuse into the transport layers, with halide ions being localized in the device electrodes.[24,43, 45–48] This effect may cause a range of problems, for example, loss of charge selectivity due to a change of the electrode work function, oxidation/corrosion, the formation of insulating layers, and the de-oxidation of doped transport layers.

Although tackling the stability has always been a main priority for perovskite researchers, the community still lacks to some extent the experimental methodologies required to quantitatively characterize mobile ions in perovskite semiconductors to overcome these limitations. For example, besides the above discussed degradation pathways which are chemical and mechanical in nature, it is not yet possible to quantitatively determine the ageing induced performance loss due to mobile ions and to differentiate these losses from those due to defects and other device and material parameters. In this regard, we have recently presented a method to determine the contribution of mobile ion-induced efficiency losses to the device performance and we have shown that the presence of mobile ions leads to moderate efficiency losses in fresh devices with low levels of apparent hysteresis (typically 1–3% absolute). The underlying mechanism of these ion-induced losses is the movement of mobile ions to the perovskite-transport layer interfaces, leading to current losses due to field screening and a reduction in charge extraction efficiency.[49]

In this work, we determine the contribution of mobile ion-induced degradation losses to the total degradation loss in the presence of external stressors for a range of different perovskite solar cells. Using *JV* measurements at different scan speeds, we first demonstrate that these losses can be directly linked to the movement of mobile ions and an increase in mobile ion density which dominates the initial performance losses of perovskite solar cells. In particular, we show that an increased mobile ion density upon prolonged illumination leads to a substantial decrease in the steady-state power conversion efficiency (PCE), mainly due to a significant reduction in short circuit current (J_{SC}) from fast to slow scan

speeds that can exceed 10 $mAcm^{-2}$. We attribute this result to increased field screening - a phenomenon that has not been previously discussed in relation to the degradation of perovskite solar cells. We also show that interfacial recombination does not increase upon ageing, yet there is an increasing mismatch between open-circuit voltage (V_{OC}) and the quasi-Fermi level splitting (QFLS) which can also be attributed to an increased accumulation of ions in the contact regions. As such, the increasing mobile ion density dominates the early ageing stages of perovskite solar cells. Finally, we show the general validity of this result for a range of different perovskite compositions, including methylammonium lead iodide ("MAPI"), a formamidinium cesium lead iodide ("CsFA"), a mixed-halide wide gap perovskite ("1.8 eV WG"), and a formamidinium-rich triple halide perovskite ("95:5 TH"). This work establishes key insights into the process of device degradation and the critical role mobile ions play therein and lays the foundation for accelerated ageing tests to predict the long-term stability of perovskite devices based on a quantitative analysis of ion-induced losses.

Results

In order to investigate the effects of illumination-induced degradation in the perovskite solar cells, we started off investigating the commonly used triple cation $Cs_{0.05}(FA_{0.83}MA_{0.17})_{0.95}Pb(I_{0.83}Br_{0.17})_3$ perovskite composition with a bandgap of 1.63 eV in a *pin*-type architecture (referred to as "83:17 TC" throughout the rest of this manuscript). The following cell architecture was used: ITO/PTAA/PFN-Br/perovskite/C_{60}/BCP/Cu, ITO is indium tin oxide, PTAA is poly[bis(4-phenyl)(2,4,6-trimethylphenyl)amine], PFN-Br is Poly({9,9-bis[30-({N,N-dimethyl}-N-ethylammonium)-propyl]-2,7-fluorene}-alt-2,7-{9,9-di-n-octylfluorene}) dibromide, and BCP is bathocuproine.[50] The cells were subjected to three different external stressors: light, heat, and electrical bias, with a focus on light-induced degradation. During the light-induced ageing, devices were exposed to 1 sun illumination at V_{OC} and cooled such that the device temperature remained at 25 C. Measurements under (MPP) maximum power point conditions are discussed further below. In Fig. 1a, the stabilized *JV* curves (wo/ hysteresis) at slow scan speeds (10 mV/s) after different illumination times under V_{OC} are exemplified. Figure 1b shows how the different device parameters change over time with ageing. In these cells, the increasing J_{SC} losses over time dominate the degradation losses although FF losses are also significant, and the V_{OC} decreases slightly as well. Based on our previous works,[49] we suspect that the increased current losses observed here might be caused by an increase in the mobile ion density in the perovskite.

In order to quantify the impact of mobile ions on the light-induced performance degradation we performed fast-hysteresis (FH) *JV* measurements at different points in time during the ageing process. While details are presented in the **Experimental methods** and in ref.[51], we note that the cell is initially hold slightly above the initial V_{OC} (prebias), followed by a reverse and forward sweep with variable frequency or scan speed. The duration of the prebias was 5x longer than the total scan time of the voltage sweep. The methodology allows us to determine the efficiency in steady state and the "ion-freeze" efficiency, which refers to the condition at which the ions are effectively immobilized when the scan rate is much

quicker than the diffusion rate.[51] The difference between slow (steady-state) and fast-scan speeds can be directly attributed to the movement of mobile ions. In the following, these losses are referred to as mobile ion-induced PCE losses. However, it should be noted that the presence of mobile ions can still affect the PCE even when they are immobilized depending on their distribution and accumulation throughout the device and at the interfaces.[51,52] This effect will be small if the ions are homogeneously distributed in the bulk at the start of the scan which is discussed further below. The results, displayed in Fig. 2a, reveal once again that the steady-state efficiency drops significantly with ageing. Conversely, the ion-freeze efficiency, determined at fast scan speeds of around 2500 V/s experiences a much smaller, almost negligible reduction. Next, we investigated the effects on each of the three *JV* metrics: the V_{OC}, J_{SC} and fill factor (FF), displayed in Fig. 2b-d. It can be seen that the illumination-induced performance losses are largely related to a drastic loss of the steady-state current output with respect to the ion-freeze J_{SC} (even more than 10 mA cm^{-2} current loss can be observed at longer aging times and in other systems). However, the V_{OC} and the FF are also affected to some extent. Furthermore, the "peak hysteresis"' i.e. the maximum difference between the PCE determined from the forward versus the reverse scan also increases significantly with aging. Overall, the remarkable difference in the PCE between the fast and slow scan speeds (Fig. 2e and **f**) shows that the dominant loss mechanism upon ageing acts more significantly at the slower timescales.

To get some understanding of the chemical changes of the perovskite film during light exposure, we performed absorption spectroscopy (**Figure S1**), X-ray diffraction (XRD) measurements on fresh and aged perovskite layers (**Figure S2**), scanning electronic microscopy (SEM) and atomic-force microscopy (AFM) measurements (**Figure S3**). As discussed in the **Supporting information**, while these measurements indicate possible changes in the morphology, these changes are considered to be relatively small on the timescale of the measurements (up to 24 h of illumination).

To generalize these findings, we then investigated the mobile ion-induced ageing loss in a range of different perovskite compositions beyond the "83:17" model system. These perovskite systems include a standard 1.6 eV methyl ammonium lead iodide $MAPbI_3$ ("MAPI"), a double cation perovskite $FA_{0.85}Cs_{15}Pb(I_{77}Br_{23})_3$ ("CsFA") with a bandgap of 1.69 eV relevant for Silicon/perovskite tandems, a wide-bandgap $Cs_{0.05}(FA_{0.60}MA_{0.40})_{0.95}Pb(I_{0.60}Br_{0.40})_3$ ("1.8 eV") relevant for all-perovskite tandems and a high performance (22% PCE) 1.57 eV formanidinum lead iodide rich ("95:5 TH") triple halide perovskite ($Cs_{0.05}(FA_{0.95}MA_{0.05})_{0.95}Pb(I_{0.95}Br_{0.05})_3$ + 20 wt% MACl). The FH results on all systems are shown in **Figure S4 – S7**. These results demonstrate that the increase of the ionic loss (L_{ion} = PCE_{fast}/PCE_{slow}) contributes significantly to total degradation loss for all systems (Fig. 3a). Moreover, we find that the reduced J_{SC} is the most important factor contributing to the ion-induced loss in all systems (**Figure S8 – S9**). Figure 3b exemplifies the large reduction of the steady-state J_{SC} after several hours of illumination (5h except for 12h in MAPI) with respect to the initial current. Figure 3c shows that the ionic losses also emerge in the much more stable 95:5 TH perovskite system which degraded to roughly 68% of its initial PCE (21%) after tracking the stabilized power output over 1630 h. The FH measurements taken initially

and after the MPP tracking reveal a nearly unchanged ion-freeze PCE, meaning that the observed power output losses can be attributed to ionic losses. We note that other factors, such as shunt formation, moisture ingress or electrode corrosion can cause an even earlier device failure, however we observe that the ionic losses are very prominent if these “extrinsic” issues are mitigated.

Having established that the ionic losses dominate the overall device degradation, we now set out to try to understand the origin of these losses by further investigating the example of the 83:17 triple cation perovskite. At this point, it is important to note that the increase of the ionic loss with aging time could be related to many other factors.[51] This is because the magnitude of the ionic loss depends on various device and material parameters for a given ion density. To identify the underlying mechanisms we now discuss, simulate, and analyse distinct scenarios. For the simulations, we used the software IonMonger[53], while the results were crossed-checked using the software SETFOS from FLUXiM.[54] In our first hypothesis, the concentration of mobile ions increases with ageing, which leads to enhanced ionic losses as shown by the simulations in Fig. 4a (see **Figure S10**, **Figure S11** and **Table S1** for the *JVs* and the corresponding PCE parameters and the simulation parameters, respectively). In this case, the increased mobile ion density causes enhanced screening of the internal field electric field in the absorber layer, which leads to a continuous reduction in charge extraction efficiency due to band flattening (**Figure S12**). The details of this loss process are discussed below in more detail. Another possible explanation for the enhanced ionic losses are degrading perovskite/transport layer interfaces with higher recombination velocities (S). As shown by the scan-rate dependent PCE in Fig. 4b, the increased recombination velocity leads to a reduced steady-state PCE and increased peak hysteresis. However, in contrast to the case of an increased ion density (Fig. 4a), the ion-freeze PCE at fast scan speeds is decreased as well. In addition, we also investigated the impact of an increased energy level offset on the FH results, as well as the impact of more bulk defects. However, we found that both (i.e. increased energetic offset and reduced bulk lifetime) lead to a parallel downshift of the scan-rate dependent PCE rather than an increase in the ionic losses, which is not consistent with the experimental results (**Figure S13**).

To further investigate the impact of potentially worsening interfaces or absorber layer quality on the enhanced ionic losses, photoluminescence (PL) measurements of different partial cell stacks were recorded as a function of illumination time. From the PL yield the quasi-Fermi level splitting (QFLS) was calculated following our previous methodology.[50,55] Surprisingly, the results displayed in Fig. 4c, suggest that the interfaces do not significantly worsen as the QFLS of all partial device stacks increases slightly over time, while the QFLS of the neat perovskite layer is nearly unchanged. Yet, the device V_{OC} decreases resulting in an increasing QFLS-eV_{OC} mismatch[55] upon ageing. While increased interfacial defects (leading to an enhanced S) are not consistent with the increased QFLS and can be likely ruled out as a dominant factor of the light-induced degradation in this cell, the increased QFLS-V_{OC} mismatch is intriguing. Although this requires further investigation, the QFLS-V_{OC} mismatch provides clues about the effect of ions at fast scan speeds. The FH simulations displayed in **Figure S14** show that if the built-in field is not offset with the prebias of the FH measurement (i.e. $V_{pre} < V_{BI}$), the V_{OC} decreases with increasing ion density. Considering that such a V_{OC} decrease (and QFLS-eV_{OC} mismatch) is observed in

various systems, the most likely scenario is that ions accumulate in an unfavourable position under open-circuit conditions (e.g. cations at the hole selective interface).[52] This is discussed further below.

Having ruled out an increased recombination velocity at the interfaces, an increased mobile-ion density seems likely to be the root-cause of the observed ageing-induced losses. In order to directly assess whether the mobile ion density increases with degradation, we performed bias assisted charge extraction (BACE) measurements and charge extraction by linearly increasing voltage (CELIV) at the same points in time when we also performed fast hysteresis measurements. Both transient charge extraction techniques can be used to estimate the mobile ion density by integrating the external current. In BACE, the cell is held under "quasi" open-circuit conditions, where the injection current equals the short-circuit current density at which the mobile ions are distributed throughout the absorber layer before the voltage is switched to 0 V, at which point the mobile ions drift to the contact layers. However, we note that if the ionic charge is larger than the electrode charge ($Q_{ion} < CV_{BI}$), the formation of zero field regions should limit the displacement of ions in excess of CV_{BI}. Thus, the CV_{BI} is expected to be a natural limit for the externally detectable ionic charge. Moreover, the ratio of the drift length of charges versus the film thickness (d_{drift}/d) limits the externally integrated charge. Therefore, the ions should be roughly homogenously distributed under the prebias condition to maximize the drift length and to avoid an underestimation of the ionic density.[56]

The results of the BACE measurements are displayed in Fig. 5a and **b**. It can be seen that the externally measured current is greatly enhanced the longer the illumination. Notably, the ionic "time of flight" in the fresh device at around 50 ms (**Figure S15**) matches nearly perfectly the scan time at the peak hysteresis observed in averaged FH on fresh devices (~50 ms). Due to the associated diffusion constant (D = 7x10^{-10} cm/s) and ionic mobility (μ = 2x10^{-8} cm^2/Vs), these results indicate that the responsible ion species are consistent with halide vacancies.[42,57] Therefore, these measurements link the transient charge extraction with the scan rate dependent *JV* results. It is also interesting to note that with prolonged ageing time, more slower species extracted which could point to A-site vacancies.[42,57] Notably, this could also explain why the peak hysteresis in the FH measurements does not shift to faster scan rates with increasing ion densities as predicted by the simulations for a given ion diffusion coefficient (Fig. 4a). As shown in Fig. 5b, by integrating the external current, a rough estimate for the ion density can be obtained. By plotting the ionic losses obtained through FH as a function of the ion density in Fig. 5c, we observe a linear dependence after an initial dwell time. It can be seen that the ion density increases significantly, even within the first hour of device ageing and reaches values over 10^{18} cm^{-3} after 20 h of ageing. Although the reason why such large densities can be obtained in BACE are not yet clear considering the above discussed limit of the detectable ionic density which requires further investigation, the obtained ion densities make sense qualitatively. As shown in Fig. 4a, the simulations can well reproduce the observed losses at the given ion densities. To highlight the effect, an ion density of 5x10^{18} cm^{-3} approximately halves the initial steady-state PCE due to enhanced ionic losses. We also note that we do not exclude some collection of ions from the side of the pixel as recently demonstrated, which could increase the ion density within the active device area.[44] Finally, with CELIV a similar picture is obtained, where the

increased mobile ion density after ageing is reflected in a strong increase in the signal on slower timescales, starting at roughly 1x10^{-4} s (**Figure S16**). Finally, we note that an increase of the ion density with increasing ageing time was also confirmed for the other studied systems (**Figure S17**), consistent with the results on the 83:17 TC cells.

In order to investigate whether the devices would age similarly under real-world conditions and to better understand the dominant factor triggering the degradation, we expanded our measurements to other ageing conditions. The FH results for degradation at elevated temperatures (75°C) in the dark (**Figure S18**), under MPP conditions at 1 sun illumination (**Figure S19**), and under electrical bias (V_{OC}) in the dark (**Figure S20**) can be seen in the SI. From these results, it becomes clear that the ion induced performance loss is a general degradation mechanism, that is also triggered by electrical bias. Nevertheless, the aging at elevated temperatures does not show the characteristic step-function like scan-rate dependent J_{SC} (Figure S18), nor displays a very large increase of the ion density on these timescales (**Figure S21**). This might point towards a different path of degradation or a slower evolution of the ionic losses. While determining the exact rates of degradation requires a much more focused investigation that goes beyond the scope of the present work, our measurements indicate that mobile ions are easily created under different stressors with different rates, in particular in the presence of electrical charges in the active layer. The fact that the increase of ionic losses behaves qualitatively similar under V_{OC}, regardless of the presence of light, but differs at elevated temperatures in the dark (and 0 V) is consistent with the interpretation that halide vacancies are generated by injected or photo-generated free holes.[45,58] In particular, it has been previously shown that iodine atoms can be oxidized and kicked out of the lattice by photogenerated holes, creating halide vacancies via $I_{\mathrm{I}}^{x} + h^{+} = I_{i}^{x} + V_{\mathrm{I}}^{+}$, where I and i refer to the regular and the interstitial lattice site, respectively and x to the neutral charge.[36,45,58] Another possible ion source is unreacted lead halide PbI_2 (Figure S2), which can decompose into metallic lead and mobile iodine under illumination.[59] Both of these mechanisms are consistent with additional X-ray photoelectron spectroscopy (XPS) measurements which reveal the presence of iodine on top of the C_{60} layer after illuminating the triple cation perovskite for approximately 10 h, demonstrating the possibility of iodine diffusion through fullerenes in line with previous reports (**Figure S22**).[24, 60–62] Moreover, we could detect iodine the perovskite film on a Si substrate that was placed ~1 mm above the sample (in N_2) during illumination, hence highlighting the egress of volatile iodine species (I_2) (**Figure S23**).

To recap, the mobile-ion induced efficiency losses observed in the FH measurements dominate the early degradation loss in the here tested halide perovskite compositions and based on various measurements such as PL and BACE, we attribute these enhanced ionic losses to an increasing ion density upon aging. Figure 6a shows a breakdown of the identified degradation losses under illumination for the 83:17 triple cation system. The J_{SC} and FF loss due to the movement of mobile ions is attributed to the field screening effect, the loss due to the QFLS-V_{OC} mismatch which is likely also a mobile-ion-induced loss, and other, yet unspecified loss processes. Figure 6b-d schematically illustrates a possible explanation of the observed J_{SC} and FF losses and the QFLS-V_{OC} mismatch. The increased ion density during the ageing

successively screens the internal (built-in) field, thus increasing the fraction of the active layer which is effectively under V_{OC} (or flat band) conditions. The formation of the zero-field region under short-circuit condition leads to an increased accumulation of electronic charges (e^- and h^+) at the hole selective interface. This charge accumulation leads in turn to enhanced recombination at the hole transport layer and in the bulk. We note that the reason why the *p*-interface is more affected than the electron-selective interface is that we consider positively charged mobile ions (halide vacancies) which screen the field at the hole transport layer. Likewise, the electron-selective interface would be stronger affected in case of a dominant negative mobile ion species. To explain the observed QFLS-V_{OC} mismatch with increased ion densities, we analyse the band diagrams at V_{OC} conditions displayed in **Figure S24** for devices with different ion densities. The graph shows that higher ion densities cause a larger electron QFL bending ($\nabla E_{\mathrm{f,e}}$) at the C_{60} interface. The bending of the electron QFL can be explained by a population inversion of electronic charges at the electron selective interface, i.e. enhanced hole accumulation and depletion of electrons, in case of an enhanced cation vacancy concentration (**Figure S25**). Considering that at V_{OC}, $\nabla E_{\mathrm{f,e}}$depends on the electron and hole conductivities and the gradient of the hole QFL, i.e. $\nabla E_{\mathrm{f,e}} = \frac{\sigma_h}{\sigma_e} \cdot \nabla E_{\mathrm{f,h}}$,[63–65] allows us to conclude that the mobile ions are likely also responsible for the observed QFLS-V_{OC} mismatch and the reduction of the V_{OC}. Finally, while there might be some small bulk recombination losses at short-circuit conditions depending on the diffusion length in the absorber layer as shown in Fig. 6d, the recombination at the interfaces increases more rapidly with enhanced cation vacancies at 0 V. Moreover, the interfacial recombination current scales faster with the applied forward bias voltage than the bulk losses, thus affecting the FF more significantly (Fig. 6d).

Conclusion

In this work, we investigated the impact of mobile ions on the ageing induced performance degradation of perovskite solar cells under different external stressors, with a focus on light-induced degradation and we thoroughly studied the underlying mechanisms behind the observed losses. We reveal a new degradation mechanism as a dominant factor in the early intrinsic degradation that has previously not been clearly identified, namely mobile-ion-induced field screening. The ionic losses manifest as a strongly reduced J_{SC}, which overall suffers most significantly under the illumination in the studied compositions while the FF and the V_{OC} are also affected by the mobile ions. With regard to the voltage losses, we found that they are caused by an increased QFLS-V_{OC} mismatch, and not due to increased interfacial defects at the perovskite-transport layer interfaces. This QFLS-V_{OC} mismatch occurs in various systems and can also be explained by an increased mobile ion density. Using different transient charge extraction techniques, we then linked the increasing current and fill factor losses upon ageing to an increase in the concentration of mobile ions in the perovskite. We showed that the increase of mobile ion concentrations upon ageing is a general degradation mechanism, which occurs also when devices are aged through exposure to other stressors, such as electrical bias. However, the ion-induced losses are more significant in the presence of free electrical charges and less under elevated temperatures, consistent with previous findings of halide vacancy generation through holes. In the future, perovskite solar cells need to be

engineered to minimize both the mobile ion densities that can be generated during ageing as well as their impact on the device performance. For example, our results highlight the key role of the hole selective interface for the initial degradation in case of large halide vacancy concentrations. By providing a crucial understanding of mobile ions and their role in the degradation, this work paves the path for the development of accelerated ageing tests based on ionic characteristics. This will allow us to identify stable conditions as well as potential mitigation routes more rapidly, which is a key for the commercialization of perovskite-based solar cells.

Declarations

Acknowledgements

We acknowledge HyPerCells (a joint graduate school of the University of Potsdam and the Helmholtz-Zentrum Berlin) and the Deutsche Forschungsgemeinschaft (DFG, German Research Foundation) - project number 423749265 and 424709669 - SPP 2196 (SURPRISE-2 and HIPSTER-PRO) as well as project number 182087777-SFB951 and MUJUPO (RI 1551/12-2) for funding. K.B. and T.R. thank the DFG (HIPSTER PRO:RI 1551/15-2), the BMBF (MOISTURE: 01DP20008 and the EU Horizon 2020 (FOXES: 951774) for funding. Y. W. acknowledges the National Natural Science Foundation of China (22179037). We also acknowledge financial support by the Federal Ministry for Economic Affairs and Energy within the framework of the 7th Energy Research Programme (P3T-HOPE, 03EE1017C). M.S. further acknowledges the Heisenberg program from the Deutsche Forschungsgemeinschaft (DFG, German Research Foundation) for funding – project number 498155101. F.L. acknowledges funding by the Volkswagen Foundation via the Freigeist Program. A.A. acknowledges support from the Welsh Government's Sêr Cymru II Rising Star through the European Regional Development Fund, Welsh European Funding Office, and Swansea University Strategic Initiative in Sustainable Advanced Materials.

Conflict of Interest

H.J.S. is co-founder and CSO of Oxford PV Ltd., a company commercializing perovskite PV technology.

Data Availability Statement

The data that support the findings of this study are available from the corresponding author upon reasonable request.

References

1. Rong, Y. *et al.* Challenges for commercializing perovskite solar cells. Science **361**, (2018).
2. Meng, L., You, J. & Yang, Y. Addressing the stability issue of perovskite solar cells for commercial applications. Nat. Commun. **9**, 1–4 (2018).

3. Ling, J. K. *et al.* A Perspective on the Commercial Viability of Perovskite Solar Cells. Sol. RRL **5**, 1–48 (2021).
4. Ruan, S. *et al.* Light induced degradation in mixed-halide perovskites. J. Mater. Chem. C **7**, 9326–9334 (2019).
5. Lang, F. *et al.* Influence of radiation on the properties and the stability of hybrid perovskites. Adv. Mater. **30**, 1–22 (2018).
6. Misra, R. K. *et al.* Temperature- and component-dependent degradation of perovskite photovoltaic materials under concentrated sunlight. J. Phys. Chem. Lett. **6**, 326–330 (2015).
7. Conings, B. *et al.* Intrinsic Thermal Instability of Methylammonium Lead Trihalide Perovskite. Adv. Energy Mater. **5**, 1–8 (2015).
8. Ouyang, Y. *et al.* Photo-oxidative degradation of methylammonium lead iodide perovskite: Mechanism and protection. J. Mater. Chem. A **7**, 2275–2282 (2019).
9. Bryant, D. *et al.* Light and oxygen induced degradation limits the operational stability of methylammonium lead triiodide perovskite solar cells. Energy Environ. Sci. **9**, 1655–1660 (2016).
10. Wang, Q. *et al.* Scaling behavior of moisture-induced grain degradation in polycrystalline hybrid perovskite thin films. Energy Environ. Sci. **10**, 516–522 (2017).
11. Salado, M. *et al.* Impact of moisture on efficiency-determining electronic processes in perovskite solar cells. J. Mater. Chem. A **5**, 10917–10927 (2017).
12. Turren-Cruz, S.-H., Hagfeldt, A. & Saliba, M. Methylammonium-free, high-performance, and stable perovskite solar cells on a planar architecture. Science **362**, 449–453 (2018).
13. Eperon, G. E. *et al.* Formamidinium Lead Trihalide: A Broadly Tunable Perovskite for Efficient Planar Heterojunction Solar Cells. Energy Environ. Sci. **7**, 982 (2014).
14. Yang, I. S. & Park, N. G. Dual Additive for Simultaneous Improvement of Photovoltaic Performance and Stability of Perovskite Solar Cell. Adv. Funct. Mater. **31**, 1–7 (2021).
15. Zhang, F. & Zhu, K. Additive Engineering for Efficient and Stable Perovskite Solar Cells. Adv. Energy Mater. **10**, 1902579 (2020).
16. Byeon, J. *et al.* Charge Transport Layer-Dependent Electronic Band Bending in Perovskite Solar Cells and Its Correlation to Light-Induced Device Degradation. ACS Energy Lett. **5**, 2580–2589 (2020).
17. Wang, F. *et al.* Highly stable perovskite solar cells with an all-carbon hole transport layer. Nanoscale **8**, 11882–11888 (2016).
18. Huang, L. & Ge, Z. Simple, Robust, and Going More Efficient: Recent Advance on Electron Transport Layer-Free Perovskite Solar Cells. Adv. Energy Mater. **9**, 1–31 (2019).
19. Li, Y., Xie, H., Lim, E. L., Hagfeldt, A. & Bi, D. Recent Progress of Critical Interface Engineering for Highly Efficient and Stable Perovskite Solar Cells. Adv. Energy Mater. **12**, 1–31 (2022).
20. Lin, Y. *et al.* Enhanced Thermal Stability in Perovskite Solar Cells by Assembling 2D/3D Stacking Structures. J. Phys. Chem. Lett. **9**, 654–658 (2018).

21. Chen, P. *et al.* In Situ Growth of 2D Perovskite Capping Layer for Stable and Efficient Perovskite Solar Cells. Adv. Funct. Mater. **28**, 1–10 (2018).
22. Grancini, G. *et al.* One-Year stable perovskite solar cells by 2D/3D interface engineering. Nat. Commun. **8**, 1–8 (2017).
23. Gahlmann, T. *et al.* Impermeable Charge Transport Layers Enable Aqueous Processing on Top of Perovskite Solar Cells. Adv. Energy Mater. **10**, 1903897 (2020).
24. Brinkmann, K. O. *et al.* Suppressed decomposition of organometal halide perovskites by impermeable electron-extraction layers in inverted solar cells. Nat. Commun. **8**, 13938 (2017).
25. Zhao, J. *et al.* Self-Encapsulating Thermostable and Air-Resilient Semitransparent Perovskite Solar Cells. Adv. Energy Mater. **7**, 1602599 (2017).
26. Arora, N. *et al.* Perovskite solar cells with CuSCN hole extraction layers yield stabilized efficiencies greater than 20%. Science **358**, 768–771 (2017).
27. Wu, S. *et al.* A chemically inert bismuth interlayer enhances long-term stability of inverted perovskite solar cells. Nat. Commun. **10**, 1161 (2019).
28. Cheacharoen, R. *et al.* Encapsulating perovskite solar cells to withstand damp heat and thermal cycling. Sustain. Energy Fuels **2**, 2398–2406 (2018).
29. Meng, W. *et al.* Revealing the strain-associated physical mechanisms impacting the performance and stability of perovskite solar cells. Joule **6**, 458–475 (2022).
30. Steele, J. A. *et al.* Thermal unequilibrium of strained black CsPbI3 thin films. Science **365**, 679–684 (2019).
31. Hoke, E. T. *et al.* Reversible Photo-induced Trap Formation in Mixed-halide Hybrid Perovskites for Photovoltaics. Chem. Sci. **6**, 613 (2015).
32. Zhang, T., Hu, C. & Yang, S. Ion Migration: A “Double-Edged Sword” for Halide-Perovskite-Based Electronic Devices. Small Methods **4**, 1900552 (2020).
33. Peña-Camargo, F. *et al.* Halide Segregation versus Interfacial Recombination in Bromide-Rich Wide-Gap Perovskite Solar Cells. ACS Energy Lett. **5**, 2728–2736 (2020).
34. Knight, A. J., Patel, J. B., Snaith, H. J., Johnston, M. B. & Herz, L. M. Trap States, Electric Fields, and Phase Segregation in Mixed-Halide Perovskite Photovoltaic Devices. Adv. Energy Mater. **10**, 1903488 (2020).
35. De Bastiani, M. *et al.* Mechanical Reliability of Fullerene/Tin Oxide Interfaces in Monolithic Perovskite/Silicon Tandem Cells. ACS Energy Lett. **7**, 827–833 (2022).
36. Kim, G. Y. *et al.* Large tunable photoeffect on ion conduction in halide perovskites and implications for photodecomposition. Nat. Mater. **17**, 445–449 (2018).
37. Walsh, A., Scanlon, D. O., Chen, S., Gong, X. G. & Wei, S. H. Self-regulation mechanism for charged point defects in hybrid halide perovskites. Angew. Chemie - Int. Ed. **54**, 1791–1794 (2015).
38. Weber, S. A. L. *et al.* How the formation of interfacial charge causes hysteresis in perovskite solar cells. Energy Environ. Sci. **11**, 2404–2413 (2018).

39. Richardson, G. *et al.* Can slow-moving ions explain hysteresis in the current-voltage curves of perovskite solar cells? Energy Environ. Sci. **9**, 1476–1485 (2016).
40. Calado, P. *et al.* Evidence for ion migration in hybrid perovskite solar cells with minimal hysteresis. Nat. Commun. **7**, 1–10 (2016).
41. Tessler, N. & Vaynzof, Y. Insights from Device Modeling of Perovskite Solar Cells. ACS Energy Lett. **5**, 1260–1270 (2020).
42. Futscher, M. H. *et al.* Quantification of ion migration in CH 3 NH 3 PbI 3 perovskite solar cells by transient capacitance measurements. Mater. Horizons **6**, 1497–1503 (2019).
43. Fu, F. *et al.* I2 vapor-induced degradation of formamidinium lead iodide based perovskite solar cells under heat-light soaking conditions. Energy Environ. Sci. **12**, 3074–3088 (2019).
44. Jacobs, D. A. *et al.* Lateral ion migration accelerates degradation in halide perovskite devices. Energy Environ. Sci. 5324–5339 (2022). doi:10.1039/d2ee02330j
45. Dunfield, S. P. *et al.* From Defects to Degradation: A Mechanistic Understanding of Degradation in Perovskite Solar Cell Devices and Modules. Adv. Energy Mater. **10**, 1–35 (2020).
46. Mei, A. *et al.* Stabilizing Perovskite Solar Cells to IEC61215:2016 Standards with over 9,000-h Operational Tracking. Joule **4**, 2646–2660 (2020).
47. Yang, T. Y., Gregori, G., Pellet, N., Grätzel, M. & Maier, J. The Significance of Ion Conduction in a Hybrid Organic-Inorganic Lead-Iodide-Based Perovskite Photosensitizer. Angew. Chemie - Int. Ed. **54**, 7905–7910 (2015).
48. Kato, Y. *et al.* Silver Iodide Formation in Methyl Ammonium Lead Iodide Perovskite Solar Cells with Silver Top Electrodes. Adv. Mater. Interfaces **2**, 2–7 (2015).
49. Thiesbrummel, J. *et al.* Universal Current Losses in Perovskite Solar Cells Due to Mobile Ions. Adv. Energy Mater. **11**, 2101447 (2021).
50. Stolterfoht, M. *et al.* Visualization and suppression of interfacial recombination for high-efficiency large-area pin perovskite solar cells. Nat. Energy **3**, 847–854 (2018).
51. Le Corre, V. M. *et al.* Quantification of Efficiency Losses Due to Mobile Ions in Perovskite Solar Cells via Fast Hysteresis Measurements. Sol. RRL **6**, 2100772 (2022).
52. Jacobs, D. A. *et al.* Hysteresis phenomena in perovskite solar cells: The many and varied effects of ionic accumulation. Phys. Chem. Chem. Phys. **19**, 3094–3103 (2017).
53. Courtier, N. E., Cave, J. M., Walker, A. B., Richardson, G. & Foster, J. M. IonMonger: a free and fast planar perovskite solar cell simulator with coupled ion vacancy and charge carrier dynamics. J. Comput. Electron. **18**, 1435–1449 (2019).
54. Aeberhard, U. *et al.* Numerical Optimization of Organic and Hybrid Multijunction Solar Cells. in *2019 IEEE 46th Photovoltaic Specialists Conference (PVSC)* 0105–0111 (IEEE, 2019). doi:10.1109/PVSC40753.2019.8980824
55. Stolterfoht, M. *et al.* The impact of energy alignment and interfacial recombination on the internal and external open-circuit voltage of perovskite solar cells. Energy Environ. Sci. **12**, 2778–2788

(2019).
56. Kniepert, J. *et al.* Reliability of charge carrier recombination data determined with charge extraction methods. J. Appl. Phys. **126**, (2019).
57. Reichert, S. *et al.* Probing the ionic defect landscape in halide perovskite solar cells. Nat. Commun. **11**, (2020).
58. Motti, S. G. *et al.* Controlling competing photochemical reactions stabilizes perovskite solar cells. Nat. Photonics **13**, 532–539 (2019).
59. Holovský, J. *et al.* Lead Halide Residue as a Source of Light-Induced Reversible Defects in Hybrid Perovskite Layers and Solar Cells. ACS Energy Lett. **4**, 3011–3017 (2019).
60. Zu, F. *et al.* Position-locking of volatile reaction products by atmosphere and capping layers slows down photodecomposition of methylammonium lead triiodide perovskite. RSC Adv. **10**, 17534–17542 (2020).
61. De Bastiani, M. *et al.* Toward Stable Monolithic Perovskite/Silicon Tandem Photovoltaics: A Six-Month Outdoor Performance Study in a Hot and Humid Climate. ACS Energy Lett. **6**, 2944–2951 (2021).
62. Sahli, F. *et al.* Fully textured monolithic perovskite/silicon tandem solar cells with 25.2% power conversion efficiency. Nat. Mater. **17**, 820–826 (2018).
63. Onno, A., Chen, C. & Holman, Z. C. Electron and hole partial specific resistances: A framework to understand contacts to solar cells. Conf. Rec. IEEE Photovolt. Spec. Conf. 2329–2333 (2019). doi:10.1109/PVSC40753.2019.8980762
64. Würfel, P. & Würfel, U. *Physics of Solar Cells: From Basic Principles to Advanced Concepts*. (Wiley-VCH, 2009).
65. Kavadiya, S. *et al.* Investigation of the Selectivity of Carrier Transport Layers in Wide-Bandgap Perovskite Solar Cells. Sol. RRL **5**, 1–9 (2021).

Figures

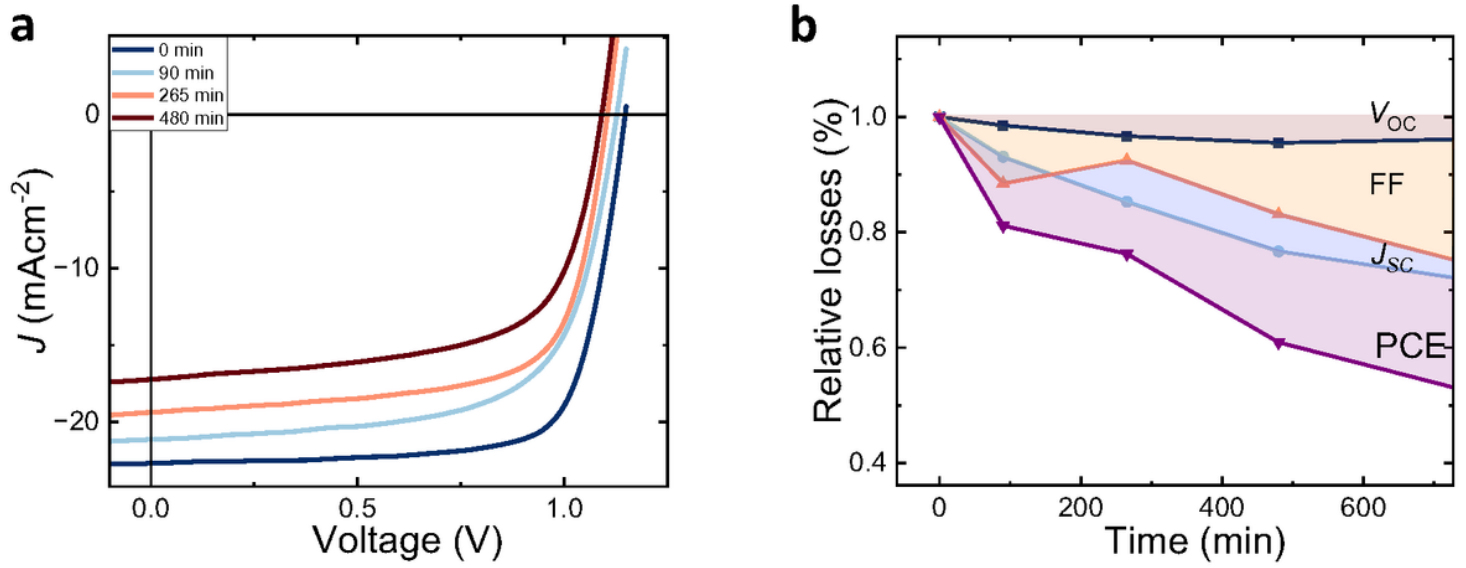

Figure 1

a Representative stabilized current-voltage (*JV*) characteristics at slow scan speeds (10 mV/s) measured on a fresh $Cs_{0.05}(FA_{0.83}MA_{0.17})_{0.95}Pb(I_{0.83}Br_{0.17})_3$ perovskite solar cell as well as after continuous illumination at V_{OC} for the specified time. **b** Relative steady-state losses of the different PCE parameters as a function of ageing time.

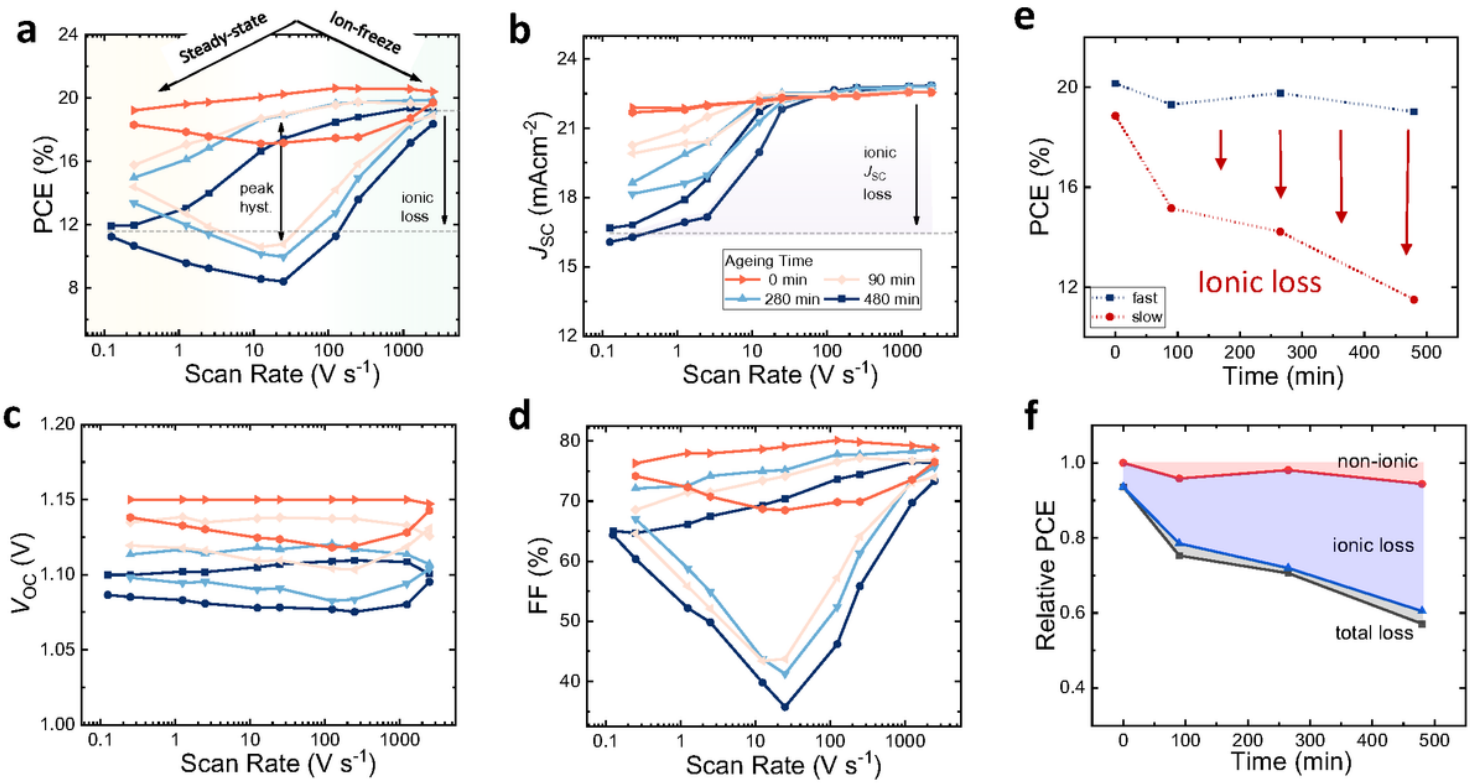

Figure 2

a The power conversion efficiency (PCE), **b** short-circuit current density (J_{SC}), **c** open-circuit voltage (V_{OC}) and **d** fill factor (FF) from current-voltage characteristics measured at different scan speeds in reverse and forward scan direction for $Cs_{0.05}(FA_{0.83}MA_{0.17})_{0.95}Pb(I_{0.83}Br_{0.17})_3$ perovskite solar cells after different ageing times. Scanning in reverse leads to a better performance metrics. **e,** Absolute and **f** relative PCE at fast and slow timescales versus aging time demonstrating the losses induced by the movement of mobile ions and small additional losses at fast scan speeds.

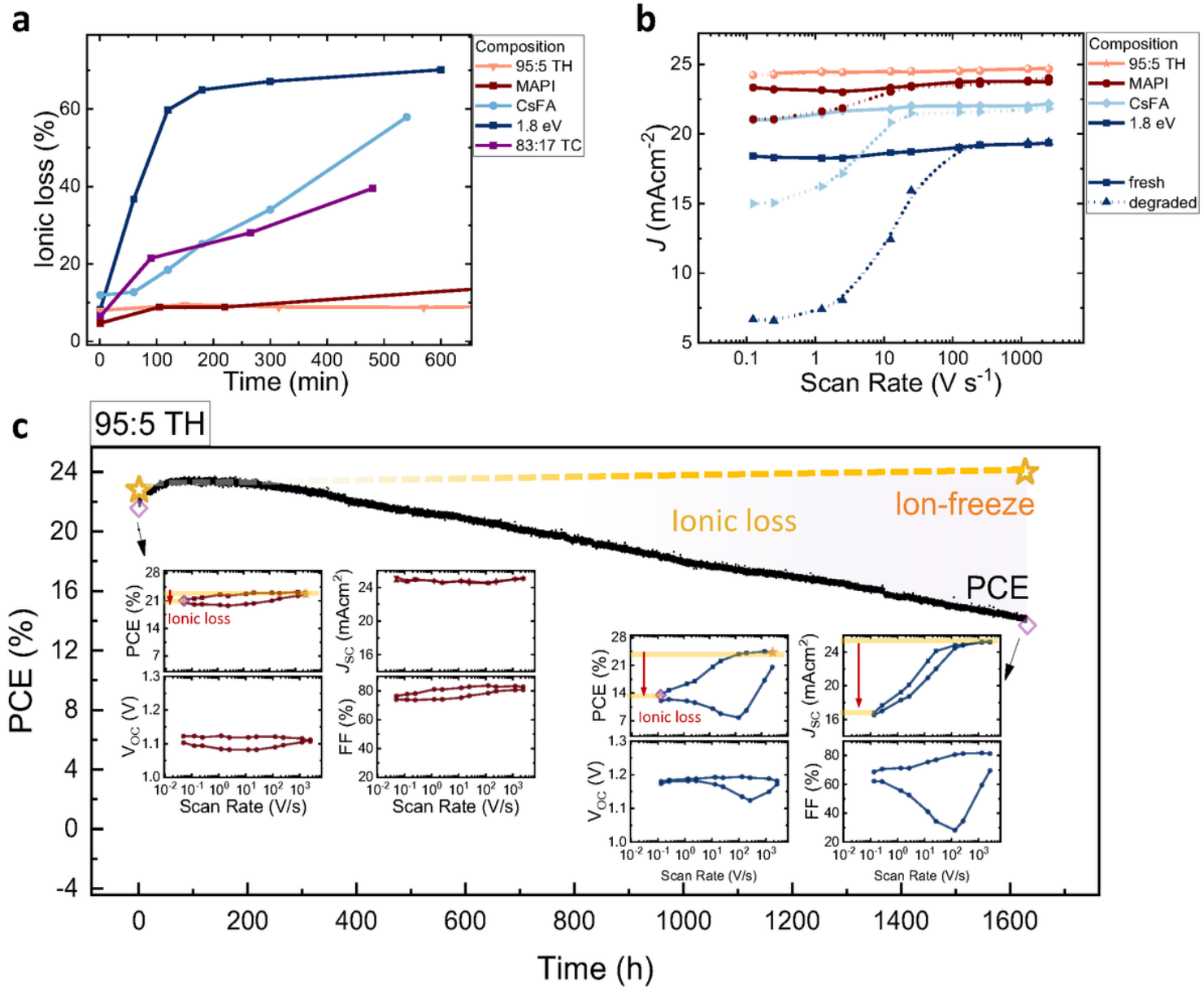

Figure 3

. a The ageing-induced relative ionic loss (L_{ion} = PCE_{fast}/PCE_{slow}) as a function of ageing time demonstrating increasing ionic losses in all systems though with varying magnitude depending on the individual composition. Highest ageing-induced ionic losses are found in the $Cs_{0.05}(FA_{0.60}MA_{0.40})_{0.95}Pb(I_{0.60}Br_{0.40})_3$ (“1.8 eV”) cell, followed by $FA_{0.85}Cs_{0.15}Pb(I_{0.77}Br_{0.23})_3$ (“CsFA”),

and 83:17 TC with the smallest losses found in $MAPbI_3$ (“MAPI”) and the $Cs_{0.05}(FA_{0.95}MA_{0.05})_{0.95}Pb(I_{0.95}Br_{0.05})_3$ + 20 wt% MACl (“95:5 TH”) cell, where the ion-induced ageing losses do not increase on these timescales. **b** The J_{SC} from *JV* curves measured at different scan speeds for fresh and aged cells after 5h hours of ageing (12h for MAPI) with additional PCE parameters shown in **Figure S4-7. c** Stabilized power point tracking on the 95:5 TH device with enhanced stability compared to the 83:17 TC reference cell. The insets shows the fast-hysteresis measurement before and after the degradation demonstrating that the observed degradation stems from ionic losses while the ion-freeze PCE remains nearly unchanged.

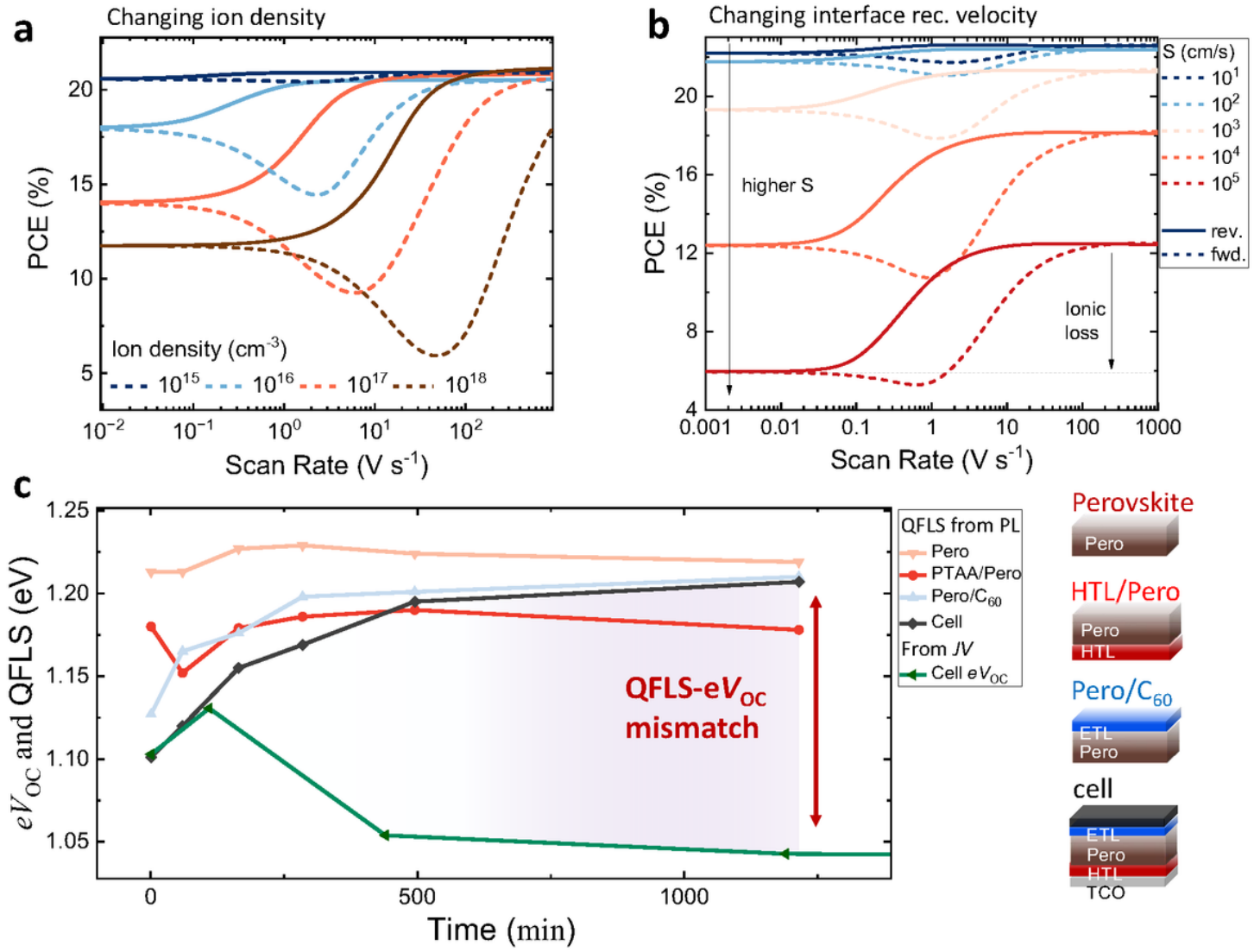

Figure 4

a The simulated PCE at different scan speeds in reverse (solid line) and forward scan (dashed line) direction for a range of different mobile ion densities. We note that we consider mobile halide vacancies in our simulations with counter ions being immobilized, however, the observed trend does not depend on the sign of the dominant mobile ion species or if there are 1 or 2 mobile species. **b** Simulated PCE from *JV* curves at different scan speeds for a range of different recombination velocities (*S*) at both perovskite-

transport layer interfaces. **c** Device V_{OC} and the QFLS measured with photoluminescence on bare triple cation films, partial and complete cell stacks as a function of illumination time.

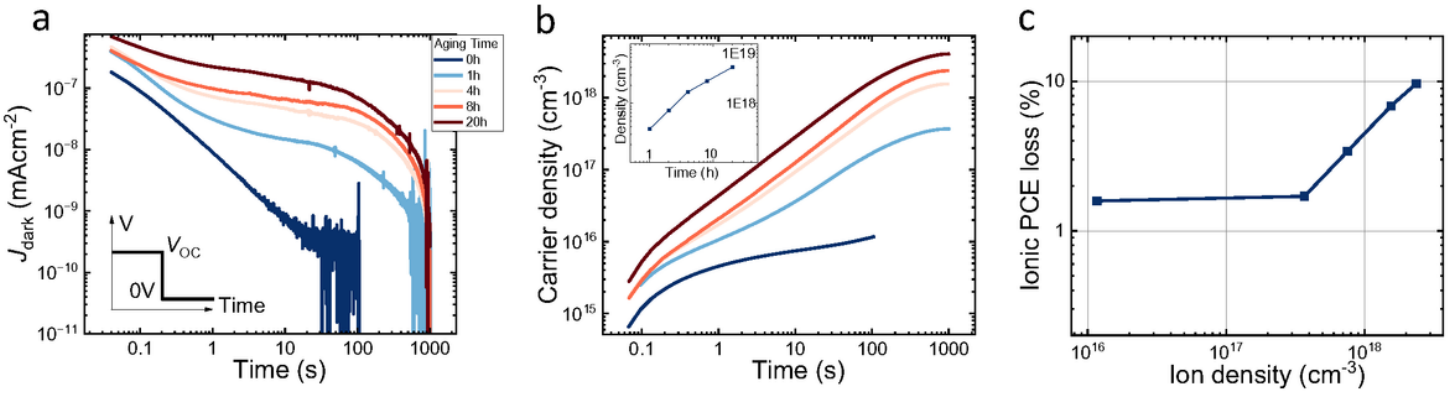

Figure 5

a Current transients from Bias Assisted Charge Extraction (BACE) measurement for both fresh and aged devices and **b** integrated charge carrier density from the transients in a. The applied voltage pulse to the device is illustrated in the inset in panel a. Considering that the capacitive (dis-) charging effect after the voltage switch and the extraction of electronic charges takes place on the µs-timescales, the contribution to the total extracted charge in these transients is expected to be nearly entirely given by mobile ions.[51] **c** The ionic loss obtained for a $Cs_{0.05}(FA_{0.83}MA_{0.17})_{0.95}Pb(I_{0.83}Br_{0.17})_3$ triple cation device as a function of the ion density reveals a linear dependence after an initial dwell aging time.

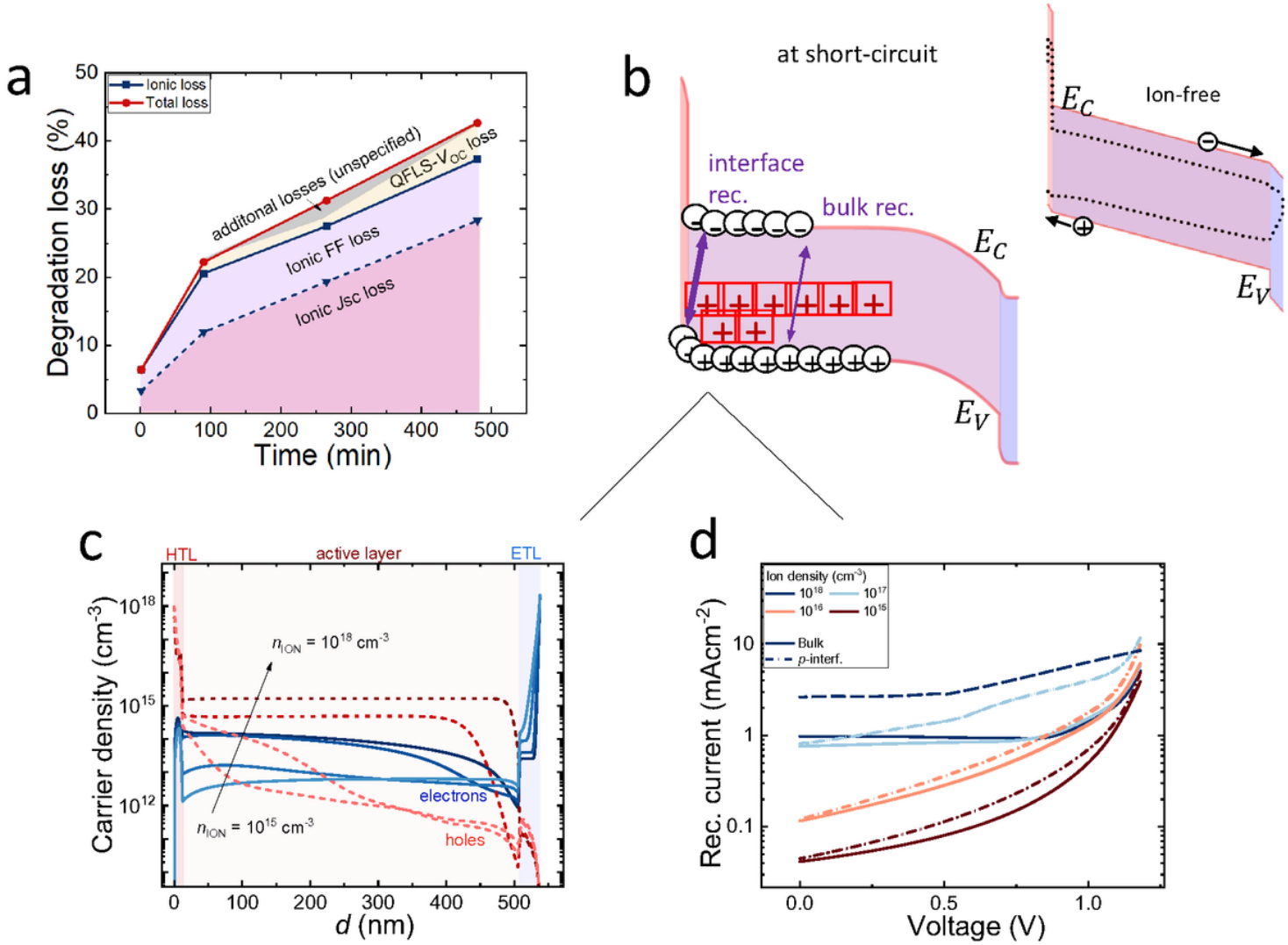

Figure 6

a Breakdown of loss processes: mobile-ion-induced J_{SC} and FF losses, mismatch of the QFLS and V_{OC} that we also attribute to accumulation of ions at the interfaces and other losses. **b** Schematic band diagram *at short-circuit conditions* highlighting the accumulation of cation vacancies at the HTL interface (*p*-interface) that leads to enhanced hole accumulation (red dashed lines) and electron accumulation (blue solid lines) close to the HTL as show in **c**. **d** The recombination current at the *p*-interface and in the bulk as a function of applied voltage for different ion densities. The inset in (b) reveals the ion-free case.

Supplementary Files

This is a list of supplementary files associated with this preprint. Click to download.

- SupplementaryInformation.docx